PCCP

Physical Chemistry Chemical Physics

rsc.li/pccp

25 YEARS ANNIVERSARY

ROYAL SOCIETY
OF **CHEMISTRY**

PAPER
Enrique M. Arpa
Excited-state antiaromaticity relief in photoactive
amine–boranes promotes transfer hydrogenation
to electron-poor olefins

PCCP
Owner Societies

Check for updates

Excited-state antiaromaticity relief in photoactive amine–boranes promotes transfer hydrogenation to electron-poor olefins†

Enrique M. Arpa 🆔

By means of DFT and multiconfigurational *ab initio* simulations, this work showcases the potential ability of photoactive amine–boranes to undergo transfer hydrogenation for the reduction of unsaturated compounds. Following absorption of UV-A light, the model amine–borane populates a low-lying triplet state. Then, the reduction of carbon–carbon double bonds proceeds through low activation barriers, one order of magnitude lower than those in the electronic ground state. The crucial role of excited-state antiaromaticity relief in facilitating this process is demonstrated by the noticeably higher barriers shown by non-triplet-antiaromatic amine–boranes for the same transformation. Overall, this work provides new design rules for developing more efficient amine–boranes for light-mediated reduction reactions.

Introduction

Transfer hydrogenation (TH) reactions are a set of transformations in which a target substrate incorporates two hydrogen atoms from a sacrificial donor, hence leading to its reduction.[1] By avoiding the use of H_2, TH offers fewer safety concerns compared to standard hydrogenation, as reactions can be conducted at atmospheric pressure and reagents do not have to be stored in pressurized gas cylinders. Among the pool of H_2 surrogates, bench-stable amine–boranes stand out for their versatility. These Lewis adducts, which consist of a 1 : 1 mixture of an amine and a borane, release H_2 under appropriate stimuli as long as both the N and B centers have at least one H atom attached to them,[2,3] a property that was later exploited for TH.[4,5] By careful selection of the parent compounds, the reactivity of amine–boranes can be controlled by the substitution pattern. While some non-catalyzed TH reactions using amine–boranes can be found in recent literature,[6–10] transition-metal-catalyzed processes are the most common examples nowadays,[11–23] employing metals ranging from expensive ones like Rh or Mo to more eco-friendly alternatives such as Ni or Fe.

However, the great thermal stability of amine–boranes is still a major hurdle to overcome. Indeed, versions of the reaction, even including some catalytic ones, require temperatures above 60 °C, sometimes up to 120 °C, to realize the

Institute of Organic Chemistry, RWTH Aachen University, 52074 Aachen, Germany.
E-mail: enrique.arpa@rwth-aachen.de

reduction of less-reactive substrates.[8–12,21,23] Instead of providing the energy necessary to overcome the activation barriers by thermal heating, a potential alternative is to deposit this energy through light irradiation. In this regard, Błyszczyk and Roure reported in 2024 the reduction of nitroarenes to anilines using Et_3N–BH_3 under 427 nm irradiation at room temperature.[24] Months later, the Leonori group employed the same amine–borane for the reduction of naphthalenes to 5,8-dihydronaphthalenes, thus preventing the formation of over-reduced decalin by-products.[25] While this reaction was carried out at room temperature as well, a more energetic light source was employed (300 nm) as naphthalenes do not absorb in the visible region of the spectrum. Moreover, due to the absence of acidic NH groups in the amine–borane, these reactions required the use of HFIP (1,1,1,3,3,3-hexafluoroisopropanol) as both the solvent and the sacrificial proton source.

While these two precedents demonstrate that photochemical reductions using amine–boranes are feasible, they also indirectly manifested one of the biggest limitations of such procedures: if the target is not photoactive and the activation barriers for the thermal reduction are high, the reactivity drops to zero. This means not only that the substrate must absorb light in the UV-visible range, but also that a long-lived excited (singlet or triplet) state must be formed following irradiation so the intermolecular TH pathway can compete with the electronic deactivation to the ground state. If there exist energetically accessible internal conversion funnels to the ground state, they lead the photoexcited population back to the ground state in a very fast and efficient way, severely hampering any excited-state reactivity. Taking olefins as example, which are a preferential target for amine–borane-mediated TH,[6,11,13,14,16,17,22] they

This journal is © the Owner Societies 2025

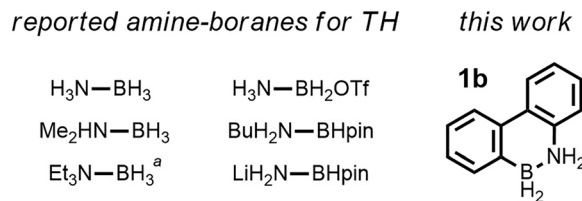*Phys. Chem. Chem. Phys.*, 2025, **27**, 18121–18127 | **18121**

Fig. 1 Some amine–boranes reported in recent literature (2010–2025) for transfer hydrogenation (TH) of unsaturated compounds (left) and the structure of the amine–borane studied in this work (right). [a] Requires HFIP as an external proton source.

Fig. 2 XMS-CASPT2/cc-pVTZ UV-vis absorption spectrum of amine–boranes **1a** (red curve) and **1b** (black curve), and the individual contributions of the three lowest-lying singlet states of **1b**. No absorption is observed above 500 nm in any case.

undergo double-bond rotations upon photoexcitation, which is the basis for molecular motors and photoswitches.[26–30]

A potential solution to this issue would be to prepare a photoactive amine–borane, so TH is triggered exclusively under light irradiation. In this way, a wider array of substrates could be reduced as the requirement of them to be photoactive or photostable is circumvented. Moreover, the excitation wavelength would remain the same for all these reactions, potentially making the set-up conditions more general. Most amine–boranes employed nowadays (Fig. 1 left) do not contain a chromophore in the UV-A-visible range (315–700 nm). This implies that it is compulsory to explore new regions of the amine–borane chemical space searching for a photoactive one. While carrying out such studies from an experimental perspective can be costly, in terms of time and waste generation, computational simulations have been successfully employed to both understand and predict the reactivity of amine–boranes in TH reactions.[15,17,18,22,25,31–37] With these precedents, the main goal of this work is, employing quantum-mechanical calculations, to ascertain if (a) it is possible to design a photoactive amine–borane with a long-lived excited state, and (b) if such photoexcited amine–borane could undergo TH to unsaturated compounds such as olefins.

Results and discussion

The first candidate as a potential photoactive amine–borane studied in this work was the 1 : 1 adduct between aniline and phenylborane (**1a**), PhH_2N-BH_2Ph. Using two phenyl groups as chromophores, the main hypothesis was that, following excitation, either the B–H or N–H bonds (or both) could be weakened due to increased $\sigma \rightarrow \pi^*$ or $\pi \rightarrow \sigma^*$ hyperconjugation effects. At the XMS-CASPT2/cc-pVTZ level of theory, it was found that the *gauche* isomer is 0.6 kcal mol^{-1} more stable than the *anti* isomer. Fig. 2 shows the semiclassical UV-vis absorption spectra of the *gauche* isomer of **1a**. All the computational details regarding the simulations carried out in this work can be found in Section S1 of the ESI.† Only one absorption band is observed in the selected 200–500 nm region of the electromagnetic spectrum, centered at 230 nm and with a low-intensity shoulder reaching 275 nm. Such an absorption profile would require the use of a Hg lamp to achieve photoexcitation (emission at 254 nm), which is highly inefficient due to its elevated cost of operation and maintenance. As an attempt to red-shift the
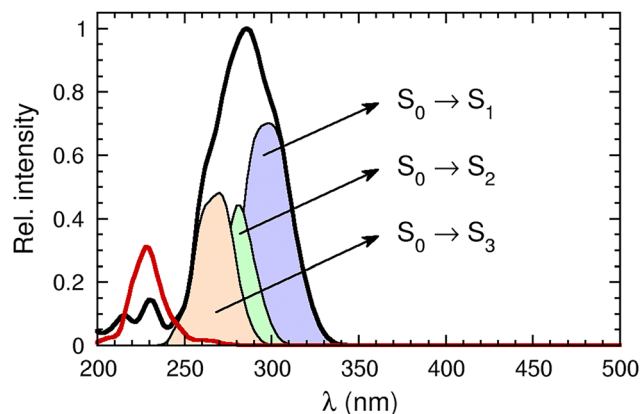
absorption spectrum, the two phenyl groups were connected leading to a phenanthrene-like structure (see Fig. 1 right), in which the carbon atoms at positions 9 and 10 have been replaced for BH_2 and NH_2 groups, respectively. Yan and cow-orkers synthesized it in 2013 as a similar amine–borane,[38] with the same structure of **1b** with the boron center protected as Bpin, suggesting that this structure should be synthetically accessible. Extending the π-conjugation throughout the two phenyl rings led to both a bathochromic (λ_{max} increases from 230 to 285 nm) and a hyperchromic (the maximum intensity acquires a 3-fold increase) shift (Fig. 2, black curve). With an absorption band that comfortably spans the UV-A region of the spectrum, reaching up to 340 nm, low-cost commercial UV LEDs could photoexcite this substrate.[25] Thus, the next steps of this work were carried out using this amine–borane.

The main absorption band of **1b** is dominated by the excitations from the ground state (S_0) to the three lowest-energy singlet $\pi\pi^*$ states (S_1, S_2, S_3). Crucially, the portion of the band in the UV-A region (315–340 nm) has the $S_0 \rightarrow S_1$ transition as its sole contributor. As it should be possible to selectively photoexcite **1b** to its S_1 state using UV-A light, only the electronic relaxation pathways that originate from this state were investigated (Fig. 3). Starting from the Franck–Condon region, a minimum in the S_1 surface can be populated, 99.7 kcal mol^{-1} above the ground-state minimum. This region is characterized by a planarization of the biphenyl structure, the dihedral angle (C5–C6–C7–C8) going from *ca.* 25° in the S_0 state to 5° in the S_1 state. From this point, an S_1/S_0 conical intersection allowing ground-state repopulation is located energetically close (107.0 kcal mol^{-1}). Accessing this crossing requires severe ring puckering at the C6 position (see Fig. S2 of the ESI† for screenshots of all the structures), which reduces the C1–C5 distance from 2.50 Å at the minimum to 1.94 Å at the crossing.

Alternatively, an S_1/T_2 crossing point is also found in the vicinity of the S_1 minimum. No transition states were found between this minimum and both crossing points. Compared to the S_1/S_0 conical intersection, this singlet–triplet crossing has a
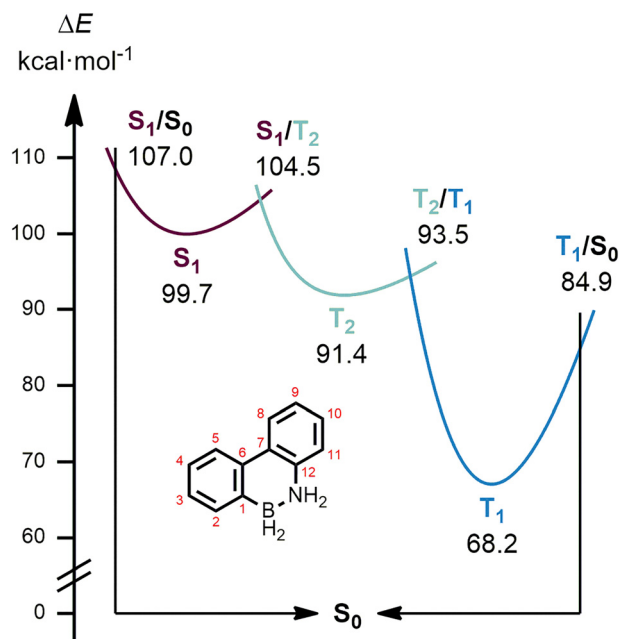
18122 | *Phys. Chem. Chem. Phys.*, 2025, **27**, 18121–18127

This journal is © the Owner Societies 2025

Fig. 3 Schematic representation of the XMS-CASPT2/cc-pVTZ singlet and triplet potential energy surfaces of **1b**. Electronic energies in kcal mol^{-1} are given relative to the ground-state minimum.

lower energy (104.5 kcal mol^{-1}) and, while there is also ring puckering at C6, it is noticeably milder (C1–C5 distance of 2.33 Å). From the S_1/T_2 crossing onwards, the ring puckering disappears and a minimum in the T_2 surface was found at 91.4 kcal mol^{-1}, making $S_1 \rightarrow T_2$ intersystem crossing (ISC) thermodynamically favored. This minimum should be short-lived, given the low energy difference that separates it from the T_2/T_1 internal conversion funnel (93.5 kcal mol^{-1}), allowing population of the more stable T_1 minimum (68.2 kcal mol^{-1}). In this region of the T_1 surface, the biphenyl core has regained planarity, the dihedral angle going from 5° in S_1 to 25° in T_2, 38° in T_2/T_1, and finally 10° in T_1. The very large energy difference that separates the T_1 minimum to the T_1/S_0 crossing point (ΔE of 16.7 kcal mol^{-1}) suggests that the T_1 state is long-lived. This energy gap comes from the harsh out-ot-plane motion of the C6–C7 bond at the crossing, which adopts a near perpendicular arrangement with respect to the C1-to-C5 ring plane. Confirming the long lifetime of this triplet state would require carrying out non-adiabatic molecular dynamics simulations, from a computational perspective, or picosecond transient absorption spectroscopy, from an experimental point of view. Without these tests, the triplet lifetime can be only roughly estimated from the static potential energy surface. Altogether, the mapping of the singlet and triplet potential energy surfaces supports the following electronic deactivation pathway for the S_1 state of **1b**: $S_1 \rightarrow S_1/T_2 \rightarrow T_2 \rightarrow T_2/T_1 \rightarrow T_1$. The population at T_1 could eventually return to the ground state *via* non-radiative decay through the T_1/S_0 crossing or by phosphorescence, emitting a 539 nm photon corresponding to the vertical energy difference between the S_0 and T_1 states at the T_1 minimum (53.0 kcal mol^{-1}).

A third option for the electronic relaxation to the ground state is to engage in a photochemical reaction with a given substrate. In the presence of an unsaturated compound, this reaction could be TH. Evidently, the reactivity towards TH will depend not only on the amine–borane but on the other reagent as well, meaning that a careful choice of a model substrate must be carried out so the results obtained can be generalized. To this end, cyclopentenone **2** was selected for several reasons. First, amine–boranes are known nucleophilic reagents as, due to the differences in electronegativity between the boron and hydrogen atoms, B–H bond cleavage tends to generate a hydride anion. For radical reactions, the reaction rates are higher if a nucleophilic reagent is put together with an electrophilic reagent, causing a stabilization of the transition state due to the so-called polar effects.[39,40] If one assumes that a similar mechanism for the TH reaction using **1b** could operate here, then this reaction would be favored with an electrophilic olefin such as **2**. Second, **2** has two electrophilic positions, C1′ and C3′ (see Fig. 4 for labelling). This means that, potentially, two distinct double bonds could be targeted for reduction, C1′–O (CO) and C2′–C3′ (CC), so information regarding chemoselectivity could be obtained as well. Third, compared to the structurally similar methyl vinyl ketone, the reduced dimensionality of the conformational space of **2** softens the computational effort.

With the aim of designing an amine–borane that only undergoes TH upon triggering with light, the activation barriers
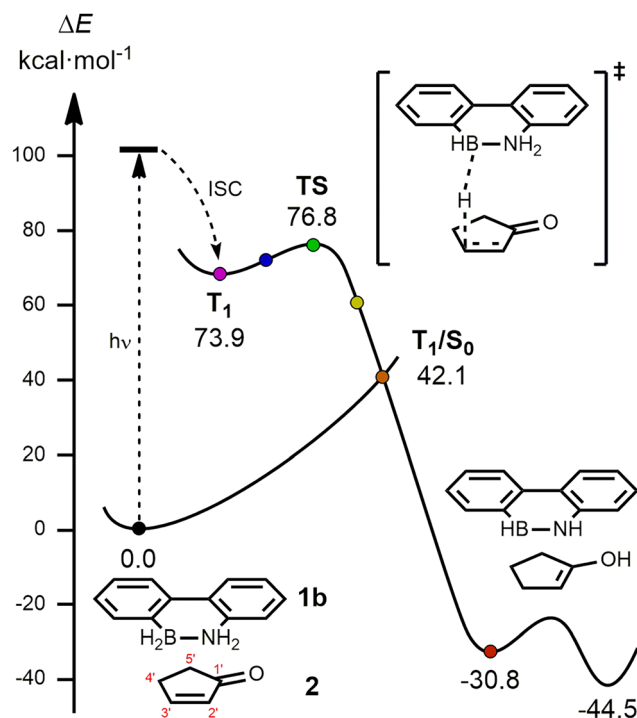

Fig. 4 M06-2X/cc-pVTZ calculated mechanism for the TH reaction from **1b** to the CC bond of **2**. Electronic energies in kcal mol^{-1} are given relative to the ground-state reaction complex. The colored points mark the points of the reaction pathway that were investigated in detail in later sections of this paper.

This journal is © the Owner Societies 2025

Phys. Chem. Chem. Phys., 2025, **27**, 18121–18127 | **18123**

in the ground state for this process should be as high as possible to prevent any background reaction. Screenshots of all the transition states for all the reactions calculated in this work can be found in Section 10 of the ESI.† The calculation of the transition states for the TH to the CC and CO bonds of **2** revealed that, in the ground state, these reactions follow a concerted, highly synchronous pathway, in which both hydrogen atoms migrate simultaneously from **1b** to **2**. Both processes are thermodynamically favored (Table 1), yet the energy barrier for the reduction of the CC bond (21.2 kcal mol^{-1}) is higher than the barrier for the CO reduction (16.6 kcal mol^{-1}). These values should be high enough so, under low-temperature conditions, ground-state reactivity could be controlled or even completely prevented. Interestingly, these activation energies are similar to those employing common amine–boranes (see Section S3 of the ESI†) such as H_3N–BH_3 (19.9 kcal mol^{-1} to CO, 26.5 kcal mol^{-1} to CC) and Me_2HN–BH_3 (22.9 kcal mol^{-1} to CO, 27.6 kcal mol^{-1} to CC), meaning that the ground-state reactivity of **1b** is comparable to that of previously described amine–boranes.

This mechanistic landscape suffers drastic changes in the T_1 triplet state depending on the followed pathway. For the reduction of the CO bond, the reaction proceeds in a similar vein as in S_0. Upon formation of the photoexcited pre-reaction complex (73.9 kcal mol^{-1} above the ground-state complex, see Sections 4 and 5 of the ESI† for more information about the formation of this complex or the use of Gibbs free energies for the energy profiles), the synchronous double hydrogen migration from **1b** to the C1′–O bond (Section S6 of the ESI†) of **2** requires surmounting an energy barrier of 17.1 kcal mol^{-1}. The reaction proceeds entirely in the triplet state, with back-ISC to S_0 taking place after the formation of the final product. The reduction of the CC bond, though, follows a unique, stepwise pathway (Fig. 4). From the pre-reaction complex, a very low energy barrier of 2.9 kcal mol^{-1} cleaves the B–H bond, causing the migration of the H atom to the C3′ position of **2**. After the transition state, a T_1/S_0 crossing point is readily found, and no additional T_1 minimum is located between this crossing and the transition state as opposed to the CO pathway. NH bond cleavage takes place in the ground state after ISC forming an enol (−30.8 kcal mol^{-1}), which then tautomerizes to the final cyclopentanone product (−44.5 kcal mol^{-1}). The large difference between the energy barriers for the CC and CO reductions in the T_1 state ($\Delta\Delta E^{\ddagger}$ = 14.2 kcal mol^{-1}) should guarantee a highly chemoselective process. Moreover, it differentiates itself

from other amine–borane-mediated TH reactions of enones that form preferentially the allylic alcohol and thus have the opposite selectivity.[7] It is also worth mentioning that the reaction between **1b** and **2** enforcing an *exo* orientation (see Section S7 of the ESI†), which neglects any dispersion interactions between the two reagents, raises the excited-state activation energy to 5.4 kcal mol^{-1}, yet it is still considerably higher than that in the ground state (27.5 kcal mol^{-1}). Thus, it is evident that the reduction of the activation energy in the triplet state does not come from any stereoelectronic effects between **1b** and **2**. Inclusion of solvent effects does not seem to have an impact on the enhanced reactivity towards TH in the T_1 state, as shown in Section 8 of the ESI† for three common solvents employed in TH reactions:[5] tetrahydrofuran, isopropanol, and acetonitrile.

Interestingly, the population of the T_1 state did not seem to have any impact on the reacting B–H bond. Geometrically, the bond length remained fixed at 1.22 Å along the full $S_1 \rightarrow T_1$ relaxation pathway described earlier, with bond compressions or elongations no larger than 0.005 Å. No substantial changes in the hyperconjugation effects were observed either, in contrast to what was postulated in the amine–borane design stage. Using M06-2X/cc-pVTZ NBO analyses, it was found that the $\sigma \rightarrow \pi^{\star}$ second-order orbital interaction energy goes from 3.66 kcal mol^{-1} in the S_0 state to 5.74 kcal mol^{-1} in the T_1 state. The increase is even smaller for the $\pi \rightarrow \sigma^{\star}$ interaction, going from 2.08 to 2.69 kcal mol^{-1}. Thus, **1b** is not intrinsically primed for TH in the T_1 state due to weakened B–H bonds. An alternative mechanism must be acting that lowers the excited-state energy barrier one order of magnitude with respect to that in the ground state.

The phenyl rings of amine–borane **1b** are aromatic in the ground state. In the triplet state, however, Hückel rules no longer apply. Instead, Baird's rules determine that π-conjugated rings with $4n + 2$ electrons become antiaromatic in their lowest-lying $^3\pi\pi^{\star}$ state.[41] The unstable nature of antiaromatic rings makes them highly reactive species. Indeed, multiple studies in recent literature have shown that relief of excited-state antiaromaticity is the driving force in proton and hydrogen transfer reactions in singlet and triplet ππ* states.[25,42–53] To investigate if excited-state antiaromaticity plays a role in lowering the energy barrier for CC reduction, the reaction pathways using two additional amine–boranes **1c** and **1d** were calculated (Fig. 5). In **1c**, the saturated C4–C5 and C8–C9 bonds mean that this amine–borane is non-aromatic in both its S_0 and T_1 states. In contrast, the cyclooctatetraene rings in **1d** make it Hückel-antiaromatic in S_0 but Baird-aromatic in T_1, thus reversing the aromatic character of **1b**. The methylene bridge in **1d**, which is not present in the other amine–boranes, was included to remove the steric clash between the rings. It is worth highlighting that these two additional amine–boranes are only used to ascertain the impact of aromaticity on the reaction from a theoretical perspective. Therefore, properties considered of relevance for **1b** such as a long triplet lifetime or synthetic accessibility are not relevant for **1c** and **1d** and were not discussed here. Using **2** as a hydrogen acceptor, the barriers for the TH to the CC bond in the S_0 and T_1 states were calculated,

Table 1 Activation ($\Delta E^{\ddagger}$) and reaction (ΔE_r) in kcal mol^{-1} for TH to the CC or CO bonds of **2** mediated by the different amine–boranes presented in this study in their ground (S_0) and triplet (T_1) states. The reaction energies in the T_1 state were calculated considering the final ground-state product complex

	$\Delta E^{\ddagger}$ in S_0	ΔE_r in S_0	$\Delta E^{\ddagger}$ in T_1	ΔE_r in T_1
1b (CO)	16.6	−25.4	17.1	−99.3
1b (CC)	21.2	−44.5	2.9	−118.4
1c (CC)	19.7	−52.0	19.6	−85.9
1d (CC)	23.9	−30.3	23.7	−53.3

18124 | *Phys. Chem. Chem. Phys.*, 2025, **27**, 18121–18127

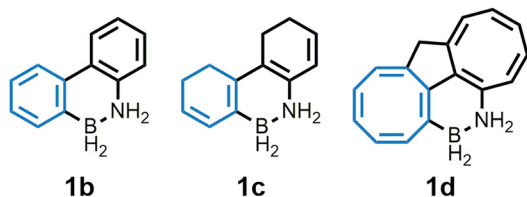This journal is © the Owner Societies 2025

Fig. 5 Additional amine–boranes tested for the TH reaction to obtain information about the role of excited-state antiaromaticity relief.

which are summarized in Table 1. With these new amine–boranes, the energy barriers are nearly identical in the two electronic states, in sheer contrast to **1b** for which the barrier decreased in almost 20 kcal mol^{-1} in the triplet state.

To assess the full impact of aromaticity, several points of the reaction coordinate were selected. These points, indicated in Fig. 4 as colored dots for the TH between **1b** and **2**, are the ground-state reaction complex (black dot), the excited-state reaction complex (purple), the transition state (green), the singlet–triplet crossing (orange), the ground-state product complex (red), and two additional dots around the transition state (blue and yellow) at which the energy gradient in the IRC was maximum. Equivalent points were selected for all the other reaction pathways in question. At these points, the NICS$_{zz}$(1) values (nucleus-independent chemical shift) were calculated for the rings marked in blue in Fig. 5, being one of the most reliable indices currently available to accurately estimate aromaticity.[54–56]

For **1c**, there are no relevant changes in aromaticity (Fig. 6), as the ring remains non-aromatic (NICS values around zero) along the complete reaction coordinate. For **1d**, the ring goes from antiaromatic (positive NICS values) to aromatic (negative values) following photoexcitation (black to purple dots). No relevant changes are observed during TH (purple to orange), and the initial antiaromaticity is restored after ISC. These results hint why the energy barriers for these two amine–boranes are similar in the S$_0$ and T$_1$ states. In contrast, for **1b**, the ring becomes antiaromatic in the T$_1$ state, but

Fig. 6 Variation of the M06-2X/cc-pVTZ NICS$_{zz}$(1) values along the reaction coordinates for the TH to the CO or CC bonds of **2** with the different amine–boranes studied in this work.

aromaticity is regained during TH. Even more, there is a clear contrast between the CO and CC pathways. For the CO pathway, the relief of antiaromaticity occurs after the transition state, while for the CC pathway it occurs before. In this way, the transition state for the reduction of the CC bond using **1b** is aromatic, which causes its stabilization and lowers the energy barrier of the process. This drastic change in aromaticity is also correctly described using other indices such as MCI (Multi-Center Index,[57] electronic) and HOMER (Harmonic Oscillator Model of Excited-state aRomaticity,[58] geometric), which are reported in Section 9 of the ESI.† Thus, it becomes evident that the reactivity of amine–borane **1b** towards TH to carbon–carbon double bonds increases in the triplet state due to excited-state antiaromaticity relief.

Conclusions

In this work, the first photoactive amine–borane for application in TH reactions has been described using state-of-the-art computational methods. Following excitation using UV-A irradiation, ISC leads to the population of a low-lying triplet state, expected to be long-lived due to the high energy gap that separates it from the triplet–singlet crossing point. This triplet state undergoes very efficient TH to carbon–carbon bonds, as proven by the low energy barrier for its reaction with a model electron-poor olefin. This barrier is much lower than the barrier for the same process in the ground state or the barriers using other amine–boranes in the triplet state. It was found that the main reason for this decrease in the energy barrier comes from the relief of excited-state antiaromaticity along the reaction coordinate, specifically right before the transition state, which stabilizes this structure. Altogether, these results demonstrate that it is possible to invert the current experimental approaches and, instead of combining a non-photoactive amine–borane with a photoactive substrate, use a photoactive amine–borane to reduce a non-photoactive substrate.

As a final remark, it is important to highlight that **1b** presented in this work should be taken as a computational proof-of-principle and not the optimal photoactive amine–borane that is ready to use in experimental studies without further optimization. It was employed as a simple structure to prove that an amine–borane can undergo highly efficient and selective TH reactions if the boryl group is covalently linked to the chromophore and a long-lived antiaromatic triplet state is populated following ISC. The results presented in this work demonstrate that any potential candidate must fulfill these two requirements. Subsequent fine tuning of the amine–borane core could help realize other desirable properties including, but not limited to, synthetic accessibility, absorption in the visible range, high ISC quantum yields, and high thermal barriers. Photoactive amine–boranes that also exhibit these features should have broader applicability compared to an unmodified **1b**, and thus it is recommended to carry out a proper screening of amine–boranes for a specific application, albeit based on the basic **1b** core.
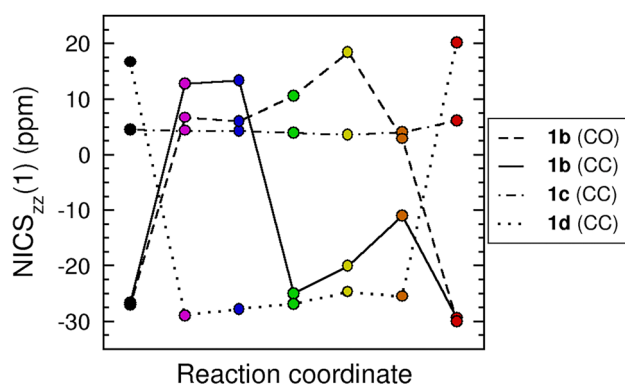
This journal is © the Owner Societies 2025

Phys. Chem. Chem. Phys., 2025, **27**, 18121–18127 | **18125**

Conflicts of interest

There are no conflicts to declare.

Data availability

The data supporting this article have been included as part of the ESI.†

Acknowledgements

References

1 D. Wang and D. Astruc, *Chem. Rev.*, 2015, **115**, 6621–6686.

2 A. Staubitz, A. P. M. Robertson and I. Manners, *Chem. Rev.*, 2010, **110**, 4079–4124.

3 A. Rossin and M. Peruzzini, *Chem. Rev.*, 2016, **116**, 8848–8872.

4 C. Faverio, M. F. Boselli, F. Medici and M. Benaglia, *Org. Biomol. Chem.*, 2020, **18**, 7789–7813.

5 S. Lau, D. Gasperini and R. L. Webster, *Angew. Chem., Int. Ed.*, 2021, **60**, 14272–14294.

6 X. Yang, T. Fox and H. Berke, *Chem. Commun.*, 2011, **47**, 2053–2055.

7 W. Xu, Y. Zhou, R. Wang, G. Wu and P. Chen, *Org. Biomol. Chem.*, 2012, **10**, 367–371.

8 S. Kumawat, S. Dey and K. Natte, *J. Org. Chem.*, 2024, **89**, 10719–10728.

9 D. Jia, Z. Ai, X. Yuan, G. Zhou, G. Zhang, P. Gao and F. Chen, *Org. Lett.*, 2025, **27**, 4294–4299.

10 X. Li, K. Wang, Y.-G. Li, Q. Zhao, Y.-N. Ma and X. Chen, *J. Am. Chem. Soc.*, 2025, **147**, 1893–1902.

11 Y. Jiang and H. Berke, *Chem. Commun.*, 2007, 3571–3573.

12 R. Barrios-Francisco and J. J. García, *Appl. Catal., A*, 2010, **385**, 108–113.

13 T.-P. Lin and J. C. Peters, *J. Am. Chem. Soc.*, 2013, **135**, 15310–15313.

14 C. E. Hartmann, V. Jurčík, O. Songis and C. S. J. Cazin, *Chem. Commun.*, 2013, **49**, 1005–1007.

15 X. Zhuang, J.-Y. Chen, Z. Yang, M. Jia, C. Wu, R.-Z. Liao, C.-H. Tung and W. Wang, *Organometallic*, 2019, **38**, 3752–3759.

16 T. M. Maier, S. Sandl, I. G. Shenderovich, A. J. von Wangelin, J. J. Weigand and R. Wolf, *Chem. – Eur. J.*, 2019, **25**, 238–245.

17 M. Espinal-Viguri, S. E. Neale, N. T. Coles, S. A. Macgregor and R. L. Webster, *J. Am. Chem. Soc.*, 2019, **141**, 572–582.

18 S.-F. Hou, J.-Y. Chen, M. Xue, M. Jia, X. Zhai, R.-Z. Liao, C.-H. Tung and W. Wang, *ACS Catal.*, 2020, **10**, 380–390.

19 C. Gelis, A. Heusler, Z. Nairoukh and F. Glorius, *Chem. – Eur. J.*, 2020, **26**, 14090–14094.

20 A. Maji, S. Gupta, D. Panja, S. Sutradhar and S. Kundu, *Organometallic*, 2023, **42**, 3385–3396.

21 C. Dewangan, S. Kumawat, T. Bhatt and K. Natte, *Chem. Commun.*, 2023, **59**, 14709–14712.

22 A. Maspero, F. Bardelli, K. F. Konidaris, M. Uboldi, C. Lucarelli, N. Schiaroli and J. G. Vitillo, *ACS Catal.*, 2024, **14**, 9594–9606.

23 T. Bhatt and K. Natte, *Org. Lett.*, 2024, **26**, 866–871.

24 P. T. Błyszczyk and B. Roure, *Synthesis*, 2024, 1–10.

25 J. Corpas, E. Rivera-Chao, E. M. Arpa, M. Gomez-Mendoza, Y. Katayama, V. A. de la Peña O'Shea, C. Bouchel, C. Jacob, P.-G. Echeverria, A. Ruffoni and D. Leonori, *Chem*, 2025, **11**, 102342.

26 B. G. Levine and T. J. Martínez, *Annu. Rev. Phys. Chem.*, 2007, **58**, 613–634.

27 T. van Leeuwen, A. S. Lubbe, P. Štacko, S. J. Wezenberg and B. L. Feringa, *Nat. Rev. Chem.*, 2017, **1**, 0096.

28 S. Kassem, T. Van Leeuwen, A. S. Lubbe, M. R. Wilson, B. L. Feringa and D. A. Leigh, *Chem. Soc. Rev.*, 2017, **46**, 2592–2621.

29 D. Cameron and S. Eisler, *J. Phys. Org. Chem.*, 2018, **31**, e3858.

30 R. Dorel and B. L. Feringa, *Chem. Commun.*, 2019, **55**, 6477–6486.

31 E. M. Leitao, N. E. Stubbs, A. P. M. Robertson, H. Helten, R. J. Cox, G. C. Lloyd-Jones and I. Manners, *J. Am. Chem. Soc.*, 2012, **134**, 16805–16816.

32 W. Xu, G. Wu, W. Yao, H. Fan, J. Wu and P. Chen, *Chem. – Eur. J.*, 2012, **18**, 13885–13892.

33 J. R. Vance, A. Schäfer, A. P. M. Robertson, K. Lee, J. Turner, G. R. Whittell and I. Manners, *J. Am. Chem. Soc.*, 2014, **136**, 3048–3064.

34 C.-Y. Peng, L. Kang, S. Cao, Y. Chen, Z.-S. Lin and W.-F. Fu, *Angew. Chem., Int. Ed.*, 2015, **127**, 15951–15955.

35 T. Wang, G. Kehr, L. Liu, S. Grimme, C. G. Daniliuc and G. Erker, *J. Am. Chem. Soc.*, 2016, **138**, 4302–4305.

36 L. Winner, W. C. Ewing, K. Geetharani, T. Dellermann, B. Jouppi, T. Kupfer, M. Schäfer and H. Braunschweig, *Angew. Chem., Int. Ed.*, 2018, **57**, 12275–12279.

37 N. Ma, M. Song, Q. Meng, C. Wei and G. Zhang, *Int. J. Quantum Chem.*, 2020, **120**, e26162.

38 Q. Jiang, D. Duan-Mu, W. Zhong, H. Chen and H. Yan, *Chem. – Eur. J.*, 2013, **19**, 1903–1907.

39 C. Rüchardt, *Angew. Chem., Int. Ed. Engl.*, 1970, **9**, 830–843.

40 A. Ruffoni, R. C. Mykura, M. Bietti and D. Leonori, *Nat. Synth.*, 2022, **1**, 682–695.

41 N. C. Baird, *J. Am. Chem. Soc.*, 1972, **94**, 4941–4948.

42 L. Gutiérrez-Arzaluz, F. Cortés-Guzmán, T. Rocha-Rinza and J. Peón, *Phys. Chem. Chem. Phys.*, 2015, **17**, 31608–31612.

43 C.-H. Wu, L. J. Karas, H. Ottosson and J. I. Wu, *Proc. Natl. Acad. Sci. U. S. A.*, 2019, **116**, 20303–20308.

18126 | *Phys. Chem. Chem. Phys.*, 2025, **27**, 18121–18127

This journal is © the Owner Societies 2025

44 B. J. Lampkin, Y. H. Nguyen, P. B. Karadakov and B. VanVeller, *Phys. Chem. Chem. Phys.*, 2019, **21**, 11608–11614.

45 L. J. Karas, C.-H. Wu, H. Ottosson and J. I. Wu, *Chem. Sci.*, 2020, **11**, 10071–10077.

46 L. J. Karas, C.-H. Wu and J. I. Wu, *J. Am. Chem. Soc.*, 2021, **143**, 17970–17974.

47 H. Kim, W. Park, Y. Kim, M. Filatov, C. H. Choi and D. Lee, *Nat. Commun.*, 2021, **12**, 5409.

48 E. M. Arpa and B. Durbeej, *Phys. Chem. Chem. Phys.*, 2022, **24**, 11496–11500.

49 J. Yan, T. Slanina, J. Bergman and H. Ottosson, *Chem. – Eur. J.*, 2023, **29**, e202203748.

50 Y. Kim, H. Kim, J. B. Son, M. Filatov, C. H. Choi, N. K. Lee and D. Lee, *Angew. Chem., Int. Ed.*, 2023, **62**, e202302107.

51 J. Draženović, C. J. Laconsay, N. Došlić, J. I. Wu and N. Basarić, *Chem. Sci.*, 2024, **15**, 5225–5237.

52 D. Xing, F. Glöcklhofer and F. Plasser, *Chem. Sci.*, 2024, **15**, 17918–17926.

53 R. Monreal-Corona, A. J. Stasyuk, M. Solà, A. Pla-Quintana and A. Poater, *Chem. Phys. Chem.*, 2024, **25**, e202400069.

54 P. V. R. Schleyer, C. Maerker, A. Dransfeld, H. Jiao and N. J. R. van Eikema Hommes, *J. Am. Chem. Soc.*, 1996, **118**, 6317–6318.

55 H. Fallad-Bagher-Shaidaei, C. S. Wannere, C. Corminboeuf, R. Puchta and P. V. R. Schleyer, *Org. Lett.*, 2006, **8**, 863–866.

56 A. Stanger, *J. Org. Chem.*, 2006, **71**, 883–893.

57 M. Giambiagi, M. S. de Giambiagi and K. C. Mundim, *Struct. Chem.*, 1990, **1**, 423–427.

58 E. M. Arpa and B. Durbeej, *Phys. Chem. Chem. Phys.*, 2023, **25**, 16763–16771.

This journal is © the Owner Societies 2025

Phys. Chem. Chem. Phys., 2025, **27**, 18121–18127 | **18127**